

A gradient-extended elastic isotropic damage model considering crack-closure

Marek Fassin^{1*}, Stephan Wulfinghoff¹ and Stefanie Reese¹

Micro Abstract

In this work an elastic isotropic damage model considering crack-closure and irreversible strains is discussed. After having introduced the model equations of the local model, results of a simple uniaxial strain controlled test on Gauss-point level are presented. Subsequently, the gradient extension of the model (micromorphic approach) is summarized briefly. Finally, the model's properties and robustness are demonstrated by means of a finite element computation of a single edge-notched plate under shear loading, where an adaptive mesh refinement is utilized.

¹Institute of Applied Mechanics, RWTH Aachen University, Aachen, Germany

*Corresponding author: marek.fassin@rwth-aachen.de

1 Model equations

1.1 Local model

In this work an elastic isotropic damage model considering crack-closure and irreversible strains is discussed. For the numerical implementation of an anisotropic damage model coupled to plasticity we refer to [3, 9]. For the discussion about damage growth for anisotropic damage models, see [10]. The here presented isotropic damage model is based on a Helmholtz free energy which consists of three parts

$$\psi = \psi_e(\hat{\boldsymbol{\varepsilon}}, D) + \psi_h(\xi_d) + \psi_p(D), \quad (1)$$

namely the elastic part, the damage hardening part and a penalty part, which ensures that the isotropic damage variable D does not exceed the value of 1. In order to model irreversible strains without additional dissipation, see [1], the shifted strain tensor $\hat{\boldsymbol{\varepsilon}} = \boldsymbol{\varepsilon} - \boldsymbol{\varepsilon}_0$ was introduced, where $\boldsymbol{\varepsilon}_0$ is the strain when crack-closure starts to be active (cf. Figure 1). Furthermore, the split of the strain in positive and negative parts is needed for the incorporation of crack-closure:

$$\hat{\boldsymbol{\varepsilon}}^+ = \sum_{i \in A} \hat{\varepsilon}_i \mathbf{n}_i \otimes \mathbf{n}_i = \sum_{i \in A} \hat{\varepsilon}_i \mathbf{N}_i, \quad A = \{i : \hat{\varepsilon}_i \geq 0\}, \quad \text{tr}^+(\hat{\boldsymbol{\varepsilon}}) = \langle \text{tr}(\hat{\boldsymbol{\varepsilon}}) \rangle, \quad (2)$$

$$\hat{\boldsymbol{\varepsilon}}^- = \sum_{i \in B} \hat{\varepsilon}_i \mathbf{n}_i \otimes \mathbf{n}_i = \sum_{i \in B} \hat{\varepsilon}_i \mathbf{N}_i, \quad B = \{i : \hat{\varepsilon}_i < 0\}, \quad \text{tr}^-(\hat{\boldsymbol{\varepsilon}}) = -\langle -\text{tr}(\hat{\boldsymbol{\varepsilon}}) \rangle, \quad (3)$$

where $\hat{\varepsilon}_i$ and \mathbf{n}_i are the eigenvalues and eigenvectors of the strain tensor $\hat{\boldsymbol{\varepsilon}}$, respectively. Further, the function $\langle x \rangle = (x + |x|)/2$ denotes the Macaulay brackets. The elastic part of the free energy is split into a positive part ψ_e^+ (corresponding to tension), where the damage is fully active and a negative part ψ_e^- (corresponding to compression) which is damaged in dependence on the

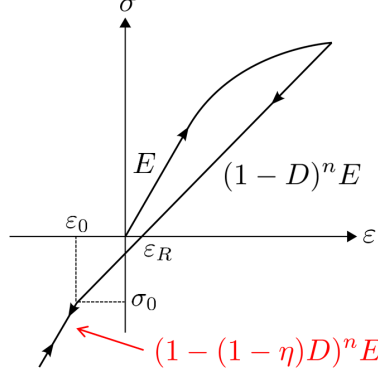


Figure 1. Schematic stress-strain diagram for loading and unloading.

crack-closure parameter η which can take values from 0 to 1:

$$\begin{aligned}
\psi_e(\hat{\varepsilon}, D) = & \underbrace{\frac{1}{2}(1-D)^n \lambda [\text{tr}^+(\hat{\varepsilon})]^2 + (1-D)^n \mu \hat{\varepsilon}^+ : \hat{\varepsilon}^+}_{\psi_e^+} \\
& + \underbrace{\frac{1}{2}(1-(1-\eta)D)^n \lambda [\text{tr}^-(\hat{\varepsilon})]^2 + (1-(1-\eta)D)^n \mu \hat{\varepsilon}^- : \hat{\varepsilon}^-}_{\psi_e^-} \\
& + \underbrace{\lambda \text{tr}(\hat{\varepsilon}) \text{tr}(\varepsilon_0) + 2\mu \hat{\varepsilon} : \varepsilon_0}_{\psi_0},
\end{aligned} \tag{4}$$

For $\eta = 0$ crack-closure is deactivated, for $\eta = 1$ crack-closure is fully active, everything in between is partially crack-closure. The energy term ψ_0 is only needed to ensure that the stress in the undeformed configuration is zero. Here, λ and μ are the Lamé parameters and n is an exponent which is either 1 or 2. The quadratic hardening energy with the hardening parameter K_1 and the penalty energy are given below as

$$\psi_h(\xi_d) = \frac{1}{2} K_1 \xi_d^2, \tag{5}$$

$$\psi_p = \frac{1}{2} H_p \langle D - D_0 \rangle^2. \tag{6}$$

By choosing a high penalty parameter H_p (e.g. 10^8) and D_0 close to one (e.g. 0.995) it is ensured that the damage variable D does not exceed the value of 1. The stress can be derived in the standard way as

$$\begin{aligned}
\boldsymbol{\sigma} = \frac{\partial \psi}{\partial \boldsymbol{\varepsilon}} = & \underbrace{(1-D)^n \lambda [\text{tr}^+(\hat{\varepsilon})] \mathbf{I} + 2(1-D)^n \mu \hat{\varepsilon}^+}_{\boldsymbol{\sigma}^+} \\
& + \underbrace{(1-(1-\eta)D)^n \lambda [\text{tr}^-(\hat{\varepsilon})] \mathbf{I} + 2(1-(1-\eta)D)^n \mu \hat{\varepsilon}^-}_{\boldsymbol{\sigma}^-} + \underbrace{\lambda \text{tr}(\varepsilon_0) \mathbf{I} + 2\mu \varepsilon_0}_{\boldsymbol{\sigma}_0}
\end{aligned} \tag{7}$$

The thermodynamic conjugate forces, namely the damage driving force Y and the damage hardening variable ξ_d , are defined as

$$\begin{aligned}
Y = -\frac{\partial \psi}{\partial D} = & \underbrace{\frac{1}{2} n (1-D)^{n-1} \lambda [\text{tr}^+(\hat{\varepsilon})]^2 + n (1-D)^{n-1} \mu \hat{\varepsilon}^+ : \hat{\varepsilon}^+}_{Y_e^+} - \underbrace{H_p \langle D - D_0 \rangle}_{Y_p} \\
& + \underbrace{\frac{1}{2} n (1-(1-\eta)D)^{n-1} (1-\eta) \lambda [\text{tr}^-(\hat{\varepsilon})]^2 + n (1-(1-\eta)D)^{n-1} (1-\eta) \mu \hat{\varepsilon}^- : \hat{\varepsilon}^-}_{Y_e^-}
\end{aligned} \tag{8}$$

$$q_d = \frac{\partial \psi}{\partial \xi_d} = K_1 \xi_d \quad (9)$$

Introducing an initial damage threshold Y_0 the damage criterion reads

$$\Phi_d = Y - (Y_0 + q_d) \leq 0. \quad (10)$$

Following the associative concept the evolution equations are given as follows

$$\dot{D} = \dot{\lambda}_d \frac{\partial \Phi_d}{\partial Y} = \dot{\lambda}_d, \quad \dot{\xi}_d = -\dot{\lambda}_d \frac{\partial \Phi_d}{\partial q_d} = \dot{\lambda}_d, \quad (11)$$

with the Kuhn Tucker conditions being

$$\dot{\lambda}_d \geq 0, \quad \phi_d \leq 0, \quad \dot{\lambda}_d \Phi_d = 0. \quad (12)$$

The secant stiffness of the material (damage state is frozen) can be calculated by

$$\begin{aligned} \frac{\partial \boldsymbol{\sigma}}{\partial \boldsymbol{\varepsilon}} = & \underbrace{(1-D)^n \lambda H_f(\text{tr}(\hat{\boldsymbol{\varepsilon}})) \mathbf{I} \otimes \mathbf{I} + (1-D)^n (\mathbb{C}_{\mu,1} + \mathbb{C}_{\mu,2})}_{(\partial \boldsymbol{\sigma} / \partial \boldsymbol{\varepsilon})^+} \\ & + \underbrace{(1 - (1-\eta)D)^n \lambda H_f(-\text{tr}(\hat{\boldsymbol{\varepsilon}})) \mathbf{I} \otimes \mathbf{I} + (1 - (1-\eta)D)^n (\mathbb{C}_{\mu,1} + \mathbb{C}_{\mu,2})}_{(\partial \boldsymbol{\sigma} / \partial \boldsymbol{\varepsilon})^-}, \end{aligned} \quad (13)$$

with

$$\mathbb{C}_{\mu,1} = 2\mu \sum_{i \in A} \mathbb{I}^s : (\mathbf{N}_i \otimes \mathbf{N}_i), \quad \mathbf{N}_i = \mathbf{n}_i \otimes \mathbf{n}_i, \mathbf{N}_{ij} = \mathbf{n}_i \otimes \mathbf{n}_j, \mathbf{N}_{ji} = \mathbf{n}_j \otimes \mathbf{n}_i, \quad (14)$$

$$\mathbb{C}_{\mu,2} = 2\mu \sum_{i \in A, j \neq i} \frac{\hat{\varepsilon}_i}{\hat{\varepsilon}_i - \hat{\varepsilon}_j} \mathbb{I}^s : \left[\frac{1}{2} (\mathbf{N}_{ij} \otimes \mathbf{N}_{ij} + \mathbf{N}_{ij} \otimes \mathbf{N}_{ji} + \mathbf{N}_{ji} \otimes \mathbf{N}_{ij} + \mathbf{N}_{ji} \otimes \mathbf{N}_{ji}) \right], \quad (15)$$

where the symmetric fourth-order identity tensor is defined as $\mathbb{I}^s = \frac{1}{2}(\delta_{ik}\delta_{jl} + \delta_{il}\delta_{jk})\mathbf{e}_i \otimes \mathbf{e}_j \otimes \mathbf{e}_k \otimes \mathbf{e}_l$.

1.2 Uniaxial strain-controlled test on Gauss-point level

In order to check the influence of the crack-closure parameter η as well as the exponent n , a uniaxial strain-controlled test in x -direction ($\varepsilon_{xx} \neq 0, \varepsilon_{yy} = \varepsilon_{zz} = 0$) is performed. This test includes loading in tension until $\varepsilon_{xx} = 1\%$ and subsequent unloading and loading in compression ($\varepsilon_{xx} < 0$) until failure. The following material parameters were used: $\lambda = 115384 \text{ N/mm}^2, \mu = 76923 \text{ N/mm}^2, Y_0 = 0.1 \text{ N/mm}^2, K_1 = 20 \text{ N/mm}^2, \boldsymbol{\varepsilon}_0 = \mathbf{0}$. Figure 2 shows the stress-strain curves for different

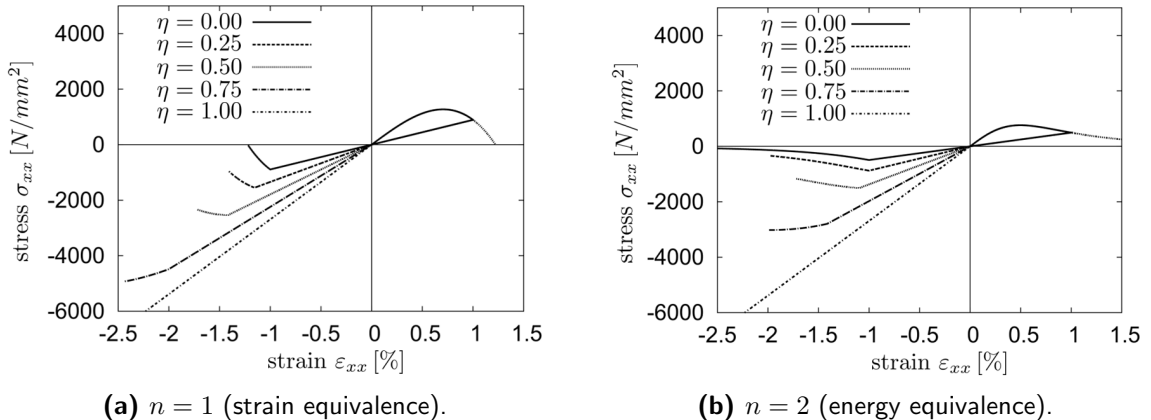


Figure 2. Uniaxial strain-controlled test with loading and unloading for different crack-closure parameters η .

values of η varying between 0 and 1. Figure 2a depicts the results for $n = 1$ which means a linear degradation of the elastic free energy by the factor $(1 - D)$. This approach is equivalent to what is commonly known as hypothesis of strain equivalence, see e.g. [5]. In the loading regime of tension no differences between the stress-strain curves for the different η can be observed. After unloading the curves branch at the the origin since crack-closure becomes active in different extend. For $\eta = 0$ no crack-closure is observed and the curve does not change its slope at the origin. It continues with an elastic part and then starts to damage again in the compression regime (later and more slowly than for $\eta = 0$) until complete failure occurs at $\sigma_{xx} = 0$. For $\eta = 0.5$ crack-closure is taken into account with 50 %. At the transition between tension and compression (origin) the stiffness increases jumpwise. The curve continues with an elastic part until damage in the compression regime is occurring. The final failure ($D=1$) takes place at nonzero stress because of the crack-closure parameter η being not equal to zero. For $\eta = 1$ crack-closure is completely active. This means that at the transition between tension and compression (origin) the initial stiffness is recovered. Furthermore, damage will not evolve under compression which means that no failure under compression occurs. Figure 2b shows the results for $n = 2$ which means a quadratic degradation of the elastic free energy by the factor $(1 - D)^2$. This approach is commonly known in the literature as hypothesis of elastic energy equivalence, see e.g. [2]. The difference compared to the first approach with $n = 1$ becomes apparent for the tension as well as for the compression regime. The $(1 - D)^2$ degradation leads to a slower damage evolution which results into a stress-strain curve which approaches zero with a horizontal tangent (see dotted lines in the tension regimes for a continued loading as well as loading in the compression regime for $\eta = 0$). As before for $n = 1$, crack-closure begins at the origin and the curves branch due to the different values/extends of crack-closure.

1.3 Gradient extension (micromorphic approach)

It is commonly known that the results of finite element computations are highly mesh dependent as soon as softening/localization takes place since the dissipation tends to zero for decreasing element size. To overcome this phenomenon a gradient extension is utilized which ensures that damage cannot localize anymore in only one element (or element row). In this work, the framework of micromorphic media according to Forest [4] is applied and implemented in analogy to Wulfinghoff and Böhlke [8]. The micromorphic approach bases on the micromorphic balance equation in the domain Ω and corresponding Neumann boundary conditions on the boundary Γ

$$\begin{aligned} \operatorname{div} \mathbf{b} - p &= 0 & \text{in } \Omega \\ \mathbf{b} \cdot \mathbf{n} &= 0 & \text{on } \Gamma \end{aligned} \quad (16)$$

Here, \mathbf{b} and p denote generalized stresses and \mathbf{n} the normal on the boundary. In order to incorporate this new balance equation the free energy of the local model from Equation 1 has to be extended by an additional micromorphic energy

$$\psi_{ext} = \psi + \psi_{micr} , \quad (17)$$

which consists of two parts

$$\psi_{micr} = \frac{A}{2} \nabla D_\chi \cdot \nabla D_\chi + \frac{H_\chi}{2} (D_\chi - D)^2 . \quad (18)$$

The first part takes into account the energy stored by the gradient of the micromorphic field variable D_χ , the second part acts as a penalty energy (with penalty parameter H_χ) which forces the micromorphic damage variable D_χ to be as close as possible to the ‘‘local’’ damage variable D . Further, the material parameter A can be expressed by $A = H_\chi l^2$, where l is the so-called internal length parameter. With the additionally introduced micromorphic energy the expressions for the generalized stresses can then be derived:

$$\mathbf{b} = \frac{\partial \psi_{micr}}{\partial \nabla D_\chi} = A \nabla D_\chi, \quad p = \frac{\partial \psi_{micr}}{\partial D_\chi} = H_\chi (D_\chi - D) . \quad (19)$$

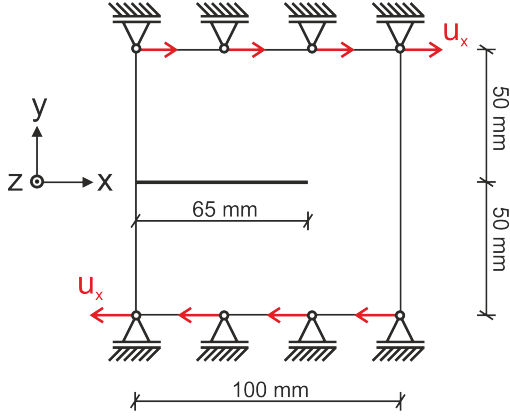


Figure 3. Single edge-notched plate: geometry, boundary conditions and loading.

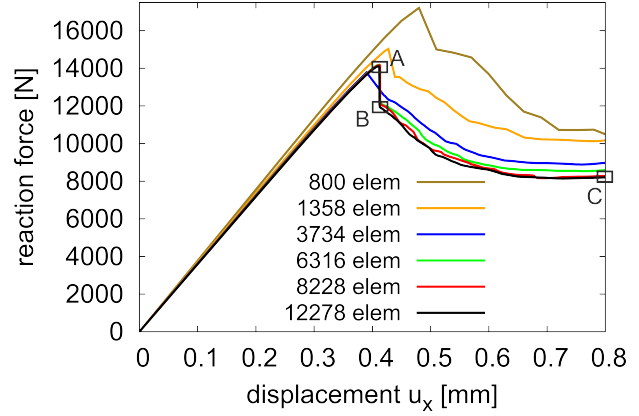


Figure 4. Force displacement curves for the six investigated meshes.

2 Numerical example

As numerical example a 2D plane strain finite element problem is considered in which a quadratic plate with a thickness of 1 mm, a side length of 100 mm and a sharp 65 mm long horizontal notch (zero width) is loaded under shear (see Figure 3). The loading is defined by the horizontal displacement u_x which is prescribed at all nodes of the top and the bottom edge of the plate. The following material parameters are used: $\lambda = 57692 \text{ N/mm}^2$, $\mu = 38462 \text{ N/mm}^2$, $n = 2$, $Y_0 = 4.0 \text{ N/mm}^2$, $K_1 = 20 \text{ N/mm}^2$, $\varepsilon_0 = \mathbf{0}$, $\eta = 1$ (crack-closure is fully active). The additional micromorphic material parameters are chosen as $H_\chi = 10^6 \text{ N/mm}^2$ and $l = 0.02 \text{ mm}$. In order to overcome snap-back situations an artificial viscosity with the value of $\theta = 0.01 \text{ N/(mm}^2\text{s)}$ is utilized. Figure 4 shows the force-displacement curves for the six investigated meshes, where the reaction force plotted on the ordinate is the sum of the reaction forces in x -direction of all nodes at the top edge. An adaptive mesh refinement strategy based on the value of the damage variable was applied. Figure 5 shows three of the six investigated meshes. The mesh with 800 elements (cf. Figure 5a) was the initial mesh on which the first remeshing was based. Further mesh refinement was then based on the finer meshes respectively. As the force-displacement curves in Figure 4 show, mesh convergence could be achieved for the mesh with 12278 elements. The three finest meshes (6316, 8228 and 12278 elements) are already very close to each other and only differ in the post peak behaviour after the sudden drop between point A and B. This drop in the force-displacement curve can be explained by the instable crack propagation between points A and B. Afterwards stable crack propagation is observed. Figure 6 illustrates the crack propagation observed in this example by means of the damage plots at points A, B and C for the mesh with 12278 elements. It should be mentioned that without considering crack-closure the damage contour plots would be symmetric with respect to the middle axis of the plate. By taking into account crack-closure (here, $\eta = 1$) the crack only evolves in the lower half of the

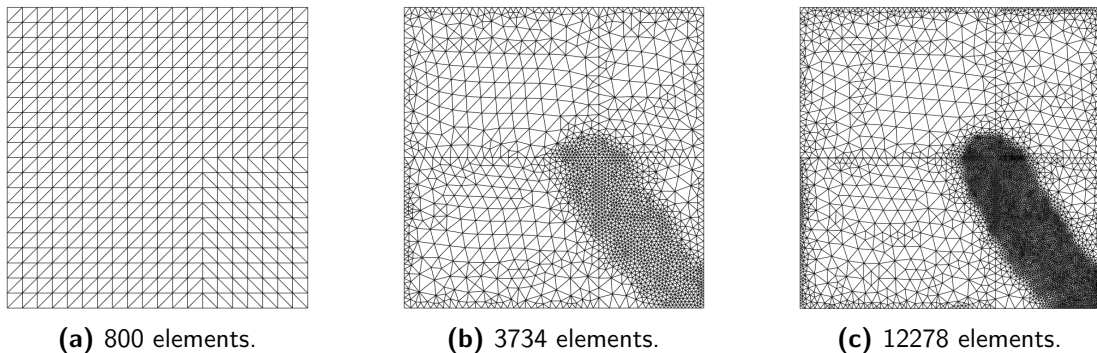


Figure 5. Meshes used for the computations.

plate which is reasonable since the upper half of the plate is dominated by compression. Similar results have been obtained by the group of Prof. Miehe using a phase field modeling of fracture approach (see, e.g. [6, 7]).

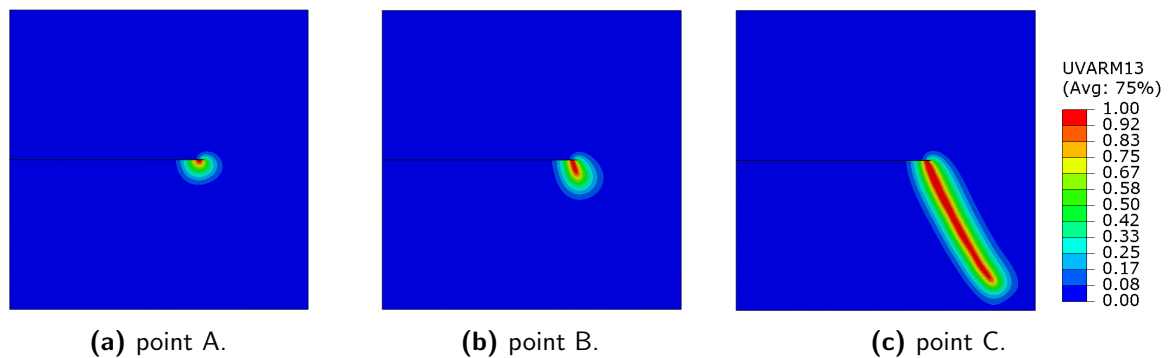


Figure 6. Damage contour plots of the crack propagation at points A,B and C in Figure 4.

Conclusions

In the present work, an elastic isotropic damage model taking into account crack-closure and irreversible strains was presented. The influence of crack-closure and the differences between strain equivalence and elastic energy equivalence were shown with simple uniaxial strain-controlled Gauss-point studies. In order to overcome the pathological mesh dependency known for this class of material models a gradient extension (micromorphic approach) was introduced and the corresponding equations were summarized briefly. In the end the model demonstrated its capability to reproduce the realistic crack path for a single edge-notched plate under shear loading. Furthermore, the employed adaptive mesh strategy proved its functionality and robustness.

Acknowledgements

The financial support of the DFG Project 'Scherschneiden kohlenstofffaserverstärkter Kunststoffe. Fertigungstechnologie und numerische Modellierung' (RE 1057/38-1) is thankfully acknowledged.

References

- [1] J.-L. Chaboche. A continuum damage theory with anisotropic and unilateral damage. *La Recherche Aéronautique*, (2):139–147, 1995.
- [2] J. Cordebois and F. Sidoroff. Damage induced elastic anisotropy. In *Mechanical Behavior of Anisotropic Solids/Comportment Mécanique des Solides Anisotropes*, pages 761–774. Springer, 1982.
- [3] M. Fassin, S. Wulfinghoff, and S. Reese. Different numerical time integration schemes for elastoplasticity coupled to anisotropic damage. In *Applied Mechanics and Materials*, volume 784, pages 217–224. Trans Tech Publ, 2015.
- [4] S. Forest. Micromorphic approach for gradient elasticity, viscoplasticity, and damage. *Journal of Engineering Mechanics*, 135(3):117–131, 2009.
- [5] J. Lemaitre. A continuous damage mechanics model for ductile fracture. *Transactions of the ASME. Journal of Engineering Materials and Technology*, 107(1):83–89, 1985.
- [6] C. Miehe, M. Hofacker, and F. Welschinger. A phase field model for rate-independent crack propagation: Robust algorithmic implementation based on operator splits. *Computer Methods in Applied Mechanics and Engineering*, 199(45):2765–2778, 2010.

- [7] C. Miehe, F. Welschinger, and M. Hofacker. Thermodynamically consistent phase-field models of fracture: Variational principles and multi-field fe implementations. *International Journal for Numerical Methods in Engineering*, 83(10):1273–1311, 2010.
- [8] S. Wulfinghoff and T. Böhlke. Equivalent plastic strain gradient crystal plasticity–enhanced power law subroutine. *GAMM-Mitteilungen*, 36(2):134–148, 2013.
- [9] S. Wulfinghoff, M. Fassin, and S. Reese. Comparison of two time-integration algorithms for an anisotropic damage model coupled with plasticity. In *Applied Mechanics and Materials*, volume 784, pages 292–299. Trans Tech Publ, 2015.
- [10] S. Wulfinghoff, M. Fassin, and S. Reese. A damage growth criterion for anisotropic damage models motivated from micromechanics. *International Journal of Solids and Structures*, 2017.